ULTRASOUND COMPRESSIVE DECONVOLUTION WITH ℓ_P-NORM PRIOR

Zhouye Chen, Ningning Zhao, Adrian Basarab, Denis Kouamé

University of Toulouse, IRIT UMR CNRS 5505, Toulouse, France

ABSTRACT

It has been recently shown that compressive sampling is an interesting perspective for fast ultrasound imaging. This paper addresses the problem of compressive deconvolution for ultrasound imaging systems using an assumption of generalized Gaussian distributed tissue reflectivity function. The benefit of compressive deconvolution is the joint volume reduction of the acquired data and the image resolution improvement. The main contribution of this work is to apply the framework of compressive deconvolution on ultrasound imaging and to propose a novel ℓ_p-norm ($1 \leq p \leq 2$) algorithm based on Alternating Direction Method of Multipliers. The performance of the proposed algorithm is tested on simulated data and compared with those obtained by a more intuitive sequential compressive deconvolution method.

***Index Terms*—** ultrasound imaging, compressive sampling, deconvolution, generalized Gaussian distribution, alternating direction method of multipliers

1. INTRODUCTION

Ultrasound (US) medical imaging has the advantages of being noninvasive, harmless, cost-effective and portable over many other imaging modalities such as X-ray Computed Tomography or Magnetic Resonance Imaging [1]. US images have a textural appearance caused by the presence of a speckle noise resulting from the interferences between the US waves backscattered by the randomly-located scatterers of the tissue being imaged. However, the limited bandwidth of the imaging transducer, the characteristics of the US propagation such as the diffraction and the imaging system tend to degrade the resolution of the US images. Thus, one of the research tracks extensively explored in the litterature is the deconvolution of US images [2–6]. Based on the first order Born approximation, these methods assume that the US radiofrequency (RF) images follow a 2D convolution model between the point spread function (PSF) and the tissue reflectivity function to be recovered [7].

More recently, a few research teams (e.g. [8–13]) evaluated the application of compressive sampling (CS) in the context of 2D and 3D US imaging. CS [14, 15] is a mathematical framework allowing to recover, via non linear optimization routines, an image from few linear measurements (below the limit imposed by the Shannon-Nyquist theorem). For this, two conditions must be fulfilled: the image must have a sparse representation in a known basis or frame and the measurement and sparifying basis must be incoherent [16]. The benefits of CS in US imaging reported by the existing approaches are the reduction of the acquired data (very useful for instance in 3D or in Doppler imaging) or/and of the acquisition time.

The direct models of both deconvolution and CS are linear models leading to ill-posed inverse problems. Thus, combining these two frameworks, leading to the so-called compressive deconvolution problem [17, 18], is a very interesting and recent research track. The benefit of compressive deconvolution is the joint volume reduction of the acquired data and the image quality improvement.

In this paper, we propose a novel scheme of compressive deconvolution and its application to US imaging. The resulting acquisition model is as follows:

$$\boldsymbol{y} = \Phi H \boldsymbol{x} + \boldsymbol{n} \tag{1}$$

where $\Phi \in \mathbb{R}^{M \times N}$ corresponds to the CS acquisition matrix composed for example by M random Gaussian vectors with ($M << N$), $H \in \mathbb{R}^{N \times N}$ is a block circulant with circulant block (BCCB) matrix related to the 2D PSF of the system, $\boldsymbol{x} \in \mathbb{R}^N$ and $\boldsymbol{n} \in \mathbb{R}^M$ represent the lexicographically ordered tissue reflectivity function and the zero-mean additive white Gaussian noise, respectively. $\boldsymbol{y} \in \mathbb{R}^M$ corresponds to the M compressed measurements of one US RF image.

The aim of this work is to estimate the tissue reflectivity function $\boldsymbol{x}$ from the compressed and blurred measurements $\boldsymbol{y}$. The solution proposed herein is based on the alternating direction method of multipliers (ADMM) [19, 20] and uses two constraints. The first one is related to CS and imposes via an l_1-norm the sparsity of the RF images in the 2D Fourier domain [9]. The second one is related to an l_p-norm [21]. Based on the assumption of Generalized Gaussian Distributed (GGD) $\boldsymbol{x}$, we employ the minimization of an l_p-norm of the tissue reflectivity function [5, 6]. The simulation results show that our method outperforms a more intuitive sequential scheme estimating firstly the blurred image and processing the deconvolution in a second step.

The remainder of the paper is organized as follows. In section 2 we formulate the compressive deconvolution problem. Section 3 details our proposed compressive deconvo-

This work is partially supported by CSC (Chinese Scholarship Council).

lution algorithm based on ADMM. Simulation results are shown in section 4 before drawing the conclusions in section 5.

2. PROBLEM FORMULATION

An intuitive idea to invert the direct model in (1) is to proceed in two sequential steps. The aim of the first step is to recover the blurred US RF image $\boldsymbol{r} = H\boldsymbol{x}$ from the compressed measurements $\boldsymbol{y}$ by solving the following optimization problem:

$$\underset{\boldsymbol{a}\in\mathbb{R}^N}{min} \|\boldsymbol{a}\|_1 + \frac{1}{2\mu}\|y - \Phi\Psi\boldsymbol{a}\|_2^2 \tag{2}$$

where μ is a parameter, $\boldsymbol{a}$ is the sparse representation of the blurred image $\boldsymbol{r}$ in the transformed domain Ψ. That is, $\boldsymbol{a} = \Psi^{-1}H\boldsymbol{x}$, where $\Psi \in \mathbb{R}^{N\times N}$ represents an orthonormal basis. Different basis have been shown to provide good results in the application of CS in US imaging, such as the wavelets, the wave atoms or the 2D Fourier basis [11] .

Once the blurred RF image recovered by minimizing the convex problem in (2), one can use an US dedicated deconvolution method to restore the tissue reflectivity function $\boldsymbol{x}$.

While the sequential approach represents the most intuitive way to solve the compressive deconvolution problem, dividing a single problem into two separate subproblems will inevitably generate larger estimation errors. Therefore, we propose herein a method to solve the CS and deconvolution problem simultaneously.

Following recent results in the US deconvolution literature [5, 6], we assume that the tissue reflectivity function $\boldsymbol{x}$ follows a GGD. Here, we are interested in shape parameters ranging from 1 to 2. Taking into account this statistical prior information for $\boldsymbol{x}$, we reformulate our compressed deconvolution problem in:

$$\underset{\boldsymbol{x}\in\mathbb{R}^N}{min} \parallel \Psi^{-1}H\boldsymbol{x} \parallel_1 + \alpha \parallel \boldsymbol{x} \parallel_p^p + \frac{1}{2\mu} \parallel y - \Phi H\boldsymbol{x} \parallel_2^2 \tag{3}$$

where α, μ are parameters, p is related to the shape parameter and $1 \leq p \leq 2$. In the next section, we propose an ADMM-based scheme to solve the inverse problem above.

3. PROPOSED ULTRASOUND COMPRESSIVE DECONVOLUTION ALGORITHM

3.1. Basics of Alternating Direction Method of Multipliers

Alternating Direction Method of Multipliers (ADMM) has been extensively studied in the areas of convex programming and variational inequalities [19]. The general optimization problem is as follows:

$$\begin{aligned} \underset{u,v}{min} \quad & f(u) + g(v) \\ s.t. \quad & Bu + Cv = b, u \in \mathcal{U}, v \in \mathcal{V} \end{aligned} \tag{4}$$

where $\mathcal{U} \subseteq \mathbb{R}^s$ and $\mathcal{V} \subseteq \mathbb{R}^t$ are given convex sets, $f : \mathcal{U} \to \mathbb{R}$ and $g : \mathcal{V} \to \mathbb{R}$ are closed convex functions; $B \in \mathbb{R}^{r\times s}$ and $C \in \mathbb{R}^{r\times t}$ are given matrices; $\boldsymbol{b} \in \mathbb{R}^r$ is a given vector.

By attaching the Lagrangian multiplier $\lambda \in \mathbb{R}^r$ to the linear constraint, the Augmented Lagrangian (AL) function of (4) is

$$\begin{aligned} \mathcal{L}(u, v, \lambda) = f(u) + g(v) - \lambda^T(Bu + Cv - b) \\ + \frac{\beta}{2} \parallel Bu + Cv - b \parallel_2^2 \end{aligned} \tag{5}$$

where $\beta > 0$ is the penalty parameter for the linear constraints to be satisfied. The standard ADMM framework follows the iterative process:

$$\begin{cases} u^{k+1} \in \underset{u\in\mathcal{U}}{argmin}\mathcal{L}(u, v^k, \lambda^k) \\ v^{k+1} \in \underset{v\in\mathcal{V}}{argmin}\mathcal{L}(u^{k+1}, v, \lambda^k) \\ \lambda^{k+1} = \lambda^k - \beta(Bu^{k+1} + Cv^{k+1} - b) \end{cases} \tag{6}$$

The advantage of ADMM is that it can split awkward intersections and objectives to easy subproblems and the iterations are comparable to those of other first-order methods. Moreover, it is relatively easy to implement.

3.2. Proposed ADMM parameterization for Ultrasound Compressive Deconvolution

In this subsection, we propose an ADMM method for solving the ultrasound compressive deconvolution problem in (3).

Using a trivial variable change, the minimization problem in (3) can be rewritten as:

$$\underset{\boldsymbol{x}\in\mathbb{R}^N}{min} \parallel \boldsymbol{w} \parallel_1 + \alpha \parallel \boldsymbol{x} \parallel_p^p + \frac{1}{2\mu} \parallel \boldsymbol{y} - A\boldsymbol{a} \parallel_2^2 \tag{7}$$

where $\boldsymbol{a} = \Psi^{-1}H\boldsymbol{x}$. Let us denote $\boldsymbol{z} = \begin{bmatrix}\boldsymbol{w}\\ \boldsymbol{x}\end{bmatrix}$, $\boldsymbol{w} = \boldsymbol{a}$ and $A = \Phi\Psi$. The reformulated problem in (7) can fit the general ADMM framework in (4) by choosing: $f(\boldsymbol{a}) = \frac{1}{2\mu} \parallel \boldsymbol{y} - A\boldsymbol{a} \parallel_2^2, g(\boldsymbol{z}) = \parallel \boldsymbol{w} \parallel_1 + \alpha \parallel \boldsymbol{x} \parallel_p^p, B = \begin{bmatrix} I_{N\times N} \\ \Psi \end{bmatrix}$, $C = \begin{bmatrix} -I_{N\times N} & \mathbf{0} \\ \mathbf{0} & -H \end{bmatrix}$ and $\boldsymbol{b} = \mathbf{0}$.

The augmented Lagrangian function of (7) is given by

$$\begin{aligned} \mathcal{L}(\boldsymbol{a}, \boldsymbol{z}, \boldsymbol{\lambda}) = f(\boldsymbol{a}) + g(\boldsymbol{z}) - \boldsymbol{\lambda}^T(B\boldsymbol{a} + C\boldsymbol{z}) \\ + \frac{\beta}{2} \parallel B\boldsymbol{a} + C\boldsymbol{z} \parallel_2^2 \end{aligned} \tag{8}$$

where $\boldsymbol{\lambda} \in \mathbb{R}^{2N}$ stands for $\boldsymbol{\lambda} = \begin{bmatrix}\boldsymbol{\lambda_1}\\ \boldsymbol{\lambda_2}\end{bmatrix}$, $\boldsymbol{\lambda_i} \in \mathbb{R}^N (i = 1, 2)$. According to the standard ADMM iterative scheme, the minimization with respect to $\boldsymbol{a}$ and $\boldsymbol{z}$ will be performed alternatively, followed by the update of $\boldsymbol{\lambda}$. More precisely, the numerical scheme for solving (8) is described in Algorithm 1. The algorithm stops when the convergence criterion $\| \boldsymbol{x}^k - \boldsymbol{x}^{k-1} \| / \| \boldsymbol{x}^{k-1} \| < 5e^{-3}$ is satisfied.

Algorithm 1 The Alternating Direction Method of Multipliers for Solving (3)

Input: $\boldsymbol{a}^0$, $\boldsymbol{\lambda}^0$, α, μ, β
Output: $\boldsymbol{x}$

1: **while** not converged **do**
2: **Step 1.** Given $\boldsymbol{a}^{k-1}$, update $\boldsymbol{w}^k$ by using the shrinkage formula:
3: $\boldsymbol{w}^k = \mathit{Shrink}_{\frac{1}{\beta}}(\boldsymbol{a}^{k-1} - \frac{\boldsymbol{\lambda_1}^{k-1}}{\beta})$
4: **Step 2.** Given $\boldsymbol{a}^{k-1}$, update $\boldsymbol{x}^k$ by using the proximal operator:
5: $\boldsymbol{x}^k = \mathit{prox}_{\alpha\gamma\|\cdot\|_p^p/\beta}\{\boldsymbol{x}^{k-1} - \gamma h'(\boldsymbol{x}^{k-1})\}$
6: **Step 3.** Given $\boldsymbol{z}^k = \begin{bmatrix}\boldsymbol{w}^k\\ \boldsymbol{x}^k\end{bmatrix}$ and $\boldsymbol{\lambda}^{k-1}$, update $\boldsymbol{a}^k$ by solving the following linear system
7: $\boldsymbol{a}^k = (\frac{1}{\mu}A^TA + \beta B^TB)^{-1}(\frac{1}{\mu}A^T\boldsymbol{y} + B^T\boldsymbol{\lambda}^{k-1} - \beta B^TC\boldsymbol{z}^k)$
8: **Step 4.** Update $\boldsymbol{\lambda}^k$ by
9: $\boldsymbol{\lambda}^k = \boldsymbol{\lambda}^{k-1} - \beta(B\boldsymbol{a}^k + C\boldsymbol{z}^k)$
10: **end while**

We solve the subproblems in Step 1 and Step 2 by using proximal operator as proposed in [22–24]. The $\boldsymbol{w}$-subproblem in Step 1 is equivalant to:

$$\min_{\boldsymbol{w}\in\mathbb{R}^N} \| \boldsymbol{w} \|_1 + \frac{\beta}{2} \| \boldsymbol{a}^{k-1} - \boldsymbol{w} - \frac{\boldsymbol{\lambda_1}^{k-1}}{\beta} \|_2^2 \tag{9}$$

The solution of (9) is given explicitly in the literature (see e.g. [25])

$$\begin{aligned}\boldsymbol{w}^k(i) = \mathit{max}\left\{|\boldsymbol{a}^{k-1}(i) - \frac{\boldsymbol{\lambda_1}^{k-1}(i)}{\beta}| - \frac{1}{\beta}, 0\right\}\\ \cdot \mathit{sign}(\boldsymbol{a}^{k-1}(i) - \frac{\boldsymbol{\lambda_1}^{k-1}(i)}{\beta})\end{aligned} \tag{10}$$

where $i \in \{1, 2, ..., N\}$, w^i denotes the intensity value of pixel i. The $\boldsymbol{x}$-subproblem in Step 2 is as follow:

$$\min_{\boldsymbol{x}\in\mathbb{R}^N} \alpha \| \boldsymbol{x} \|_p^p - \boldsymbol{\lambda_2}^{k-1^T}(\Psi\boldsymbol{a}^{k-1} - H\boldsymbol{x}) + \frac{\beta}{2} \| \Psi\boldsymbol{a}^{k-1} - H\boldsymbol{x} \|_2^2 \tag{11}$$

Denoting by $h(\boldsymbol{x}) = \frac{1}{2} \| \Psi\boldsymbol{a}^{k-1} - H\boldsymbol{x} - \frac{\boldsymbol{\lambda_2}^{k-1}}{\beta} \|_2^2$, we approximate $h(\boldsymbol{x})$ by

$$h'(\boldsymbol{x}^{k-1})(\boldsymbol{x} - \boldsymbol{x}^{k-1}) + \frac{1}{2\gamma} \| \boldsymbol{x} - \boldsymbol{x}^{k-1} \|_2^2 \tag{12}$$

where $\gamma > 0$ is a proximal parameter and $h'(\boldsymbol{x}^{k-1})$ is the gradient of $h(\boldsymbol{x})$ when $\boldsymbol{x} = \boldsymbol{x}^{k-1}$, which is equal to

$$h'(\boldsymbol{x}^{k-1}) = H^T(H\boldsymbol{x}^{k-1} - \Psi\boldsymbol{a}^{k-1} - \frac{\boldsymbol{\lambda_2}^{k-1}}{\beta}) \tag{13}$$

We should note that the proximal operator associated to $\| \cdot \|_p^p$ has been given in [25]. Herein, we use Newton's method to obtain its numerical solution.

In Step 3, the update of $\boldsymbol{a}$ is written in the form of solving an $N \times N$ linear system or inverting an $N \times N$ matrix. However, since the sparse basis Ψ is orthogonal, it can be reduced to solving a smaller $M \times M$ linear system or inverting an $M \times M$ matrix by Sherman-Morrison-Woodbury formula [26]:

$$(\beta_1 I_N + \beta_2 A^TA)^{-1} = \frac{1}{\beta_1} I_N - \frac{\beta_2}{\beta_1} A^T(\beta_1 I_M + \beta_2 AA^T)^{-1}A \tag{14}$$

where $I_N \in \mathbb{R}^{N\times N}$ and $I_M \in \mathbb{R}^{M\times M}$ are identity matrices. In this paper, we considered the compressive sampling matrix Φ as Structurally Random Matrix (SRM) [27]. Therefore, A was formed by randomly taking a subset of rows from orthonormal transform matrices, that is, $AA^T = I_M$. As a consequence, there is no need to solve a linear system and the main computational cost becomes two matrix-vector multiplications per iteration.

4. SIMULATION RESULTS

In this section we evaluate the performance of the proposed compressive deconvolution algorithm for synthetic ultrasound data against a sequential resolution processing separately the CS reconstruction and the deconvolution. For the sequential approach, YALL1 [28] was used to process the CS reconstruction from (2), while the deconvolution was done using an ℓ_p-norm minimization. To solve this minimization problem, we also used one of the parameterizations of ADMM to split the ℓ_p-norm term and the quadratic term, then solved them separately and iteratively.

The ultrasound data in Figure 1 and Figure 2 were simulated by 2D convolution between known PSFs and reflectivity images. For the first simulated image, the PSF was generated with Field II [29] corresponding to a 3.5 MHz linear probe, sampled in the axial direction at 20 MHz. For the simulated kidney image, the PSF was also generated with Field II [29]

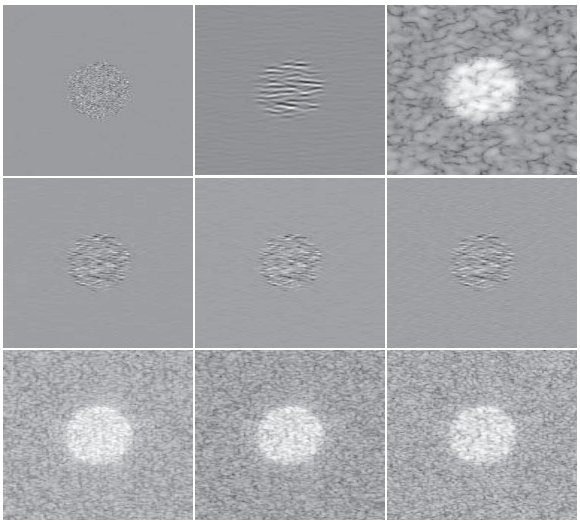

Fig. 1: The 1^{st} row represents the tissue reflectivity function, the ultrasound RF image and the corresponding B-mode image (obtained after envelope detection and log-compression from the RF image) from left to right; The 2^{nd} row depicts the compressive deconvolution results obtained with the proposed method for SNR=40dB and for CS ratios of 80%,60% and 40% respectively; The 3^{rd} row shows the corresponding B-mode images of the results in the 2^{nd} row.

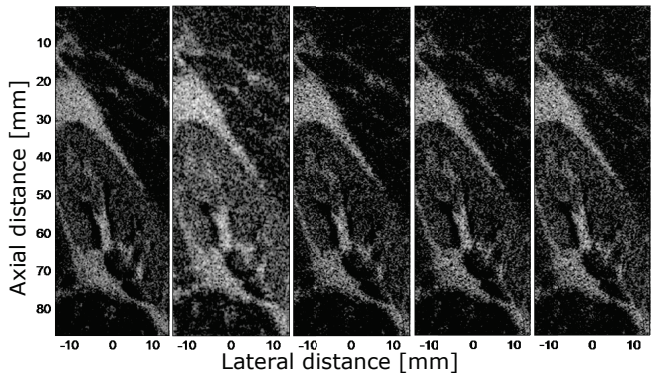

Fig. 2: Simulated kidney image and its compressive deconvolution results for SNR=40dB. From left to right, the tissue reflectivity function, the B-mode image and the compressive deconvolution results for CS ratios of 80%, 60% and 40% respectively.

corresponding to a 4 MHz central frequency and a axial sampling frequency of 40 MHz. The amplitudes of the scatters in these two reflectivity images are random variables distributed according to GGD with the shape parameter set to 1.5. The number of scatterers was considered sufficiently large to ensure fully developed speckle.

The variables $\boldsymbol{a}^0$ and $\boldsymbol{\lambda}^0$ were initialized to zeros vector and image. The rest of the hyperparameters, α, μ, β and γ, were set to their best possible values by cross-validation. For the results in Figure 1, the parameters were set to $\{\alpha, \mu, \beta, \gamma\} = \{1e-6, 1e-3, 1e-3, 1e-1\}$ and for those in Figure 2, $\{\alpha, \mu, \beta, \gamma\} = \{1e-5, 5e-3, 1e-4, 2e-4\}$.

Figure 1 and Figure 2 show a series of compressive deconvolution results for the two tested data sets, for various CS ratios and for a SNR of 40dB. Quantitative results are shown in Table 1 and Table 2 and allow the comparison between the proposed method and the sequential approach. Three metrics were employed: the Blurred-PSNR (B-PSNR) (defined and used in [17]), the Blurred-Structural Similarity (B-SSIM, defined in the same manner as B-PSNR) and the Structural Similarity (SSIM) . Ten experiments were conducted for each CS ratio. We may remark that in all cases our approach provides better reults than the sequential scheme. We should remark that in both cases the same priors were used for the CS reconstruction and for the deconvolution.

Table 1: Quatitative results for US image in Figure 1

	CS ratio	80%	60%	40%	20%
proposed	B-PSNR	52.33	47,28	40,65	28,97
	B-SSIM	99.41	98.27	93.24	48.72
	SSIM	72.52	65.06	43.74	22.40
sequential	B-PSNR	49,25	40,98	31,90	22,34
	B-SSIM	98.91	93.37	64.20	23.84
	SSIM	70.93	55.72	36.82	20.75

Table 2: Quatitative results for US image in Figure 2

	CS ratio	80%	60%	40%	20%
proposed	B-PSNR	73.75	66.98	52.38	52.12
	B-SSIM	100.0	99.99	99.64	79.11
	SSIM	60.25	59.06	52.80	26.23
sequential	B-PSNR	36.46	29.60	25.90	23.87
	B-SSIM	88.36	64.31	44.88	32.37
	SSIM	39.89	40.89	28.02	18.32

5. CONCLUSIONS

In this paper, we firstly presented a compressive deconvolution framework for ultrasound imaging systems. Then we developed a compressive deconvolution algorithm based on Alternating Direction Method of Multipliers (ADMM). Based on the assumption of generalized Gaussian distributed tissue refelectivity function, our method uses an ℓ_p-norm minimization for p between 1 and 2. The results obtained on simulated ultrasound images are promising and clearly show that the proposed simutaneously compressive deconvolution scheme performed better than the typical sequential approach. Future work will include the study of medical CS reconstruction algorithms such as [30], the automatic estimation of p for the

ℓ_p-norm, the comparison with other existing methods such as [17] and experiments on clinical data.

References

[1] T. L. Szabo, *Diagnostic ultrasound imaging: inside out*. Academic Press, 2004.

[2] T. Taxt and J. Strand, "Two-dimensional noise-robust blind deconvolution of ultrasound images," *Ultrasonics, Ferroelectrics and Frequency Control, IEEE Transactions on*, vol. 48, no. 4, pp. 861–866, 2001.

[3] O. Michailovich and A. Tannenbaum, "Blind deconvolution of medical ultrasound images: A parametric inverse filtering approach," *IEEE transactions on image processing: a publication of the IEEE Signal Processing Society*, vol. 16, no. 12, p. 3005, 2007.

[4] R. Morin, S. Bidon, A. Basarab, and D. Kouamé, "Semi-blind deconvolution for resolution enhancement in ultrasound imaging." in *ICIP*, 2013, pp. 1413–1417.

[5] N. Zhao, A. Basarab, D. Kouamé, and J.-Y. Tourneret, "Restoration of ultrasound images using a hierarchical bayesian model with a generalized gaussian prior," in *in Proc. Int. Conf. Image Process.(ICIP2014), Paris, France*, 2014.

[6] M. Alessandrini, S. Maggio, J. Porée, L. De Marchi, N. Speciale, E. Franceschini, O. Bernard, and O. Basset, "A restoration framework for ultrasonic tissue characterization," *Ultrasonics, Ferroelectrics, and Frequency Control, IEEE Transactions on*, vol. 58, no. 11, pp. 2344–2360, 2011.

[7] J. A. Jensen, J. Mathorne, T. Gravesen, and B. Stage, "Deconvolution of in vivo ultrasound b-mode images," *Ultrasonic Imaging*, vol. 15, no. 2, pp. 122–133, 1993.

[8] A. Achim, B. Buxton, G. Tzagkarakis, and P. Tsakalides, "Compressive sensing for ultrasound rf echoes using a-stable distributions," in *Engineering in Medicine and Biology Society (EMBC), 2010 Annual International Conference of the IEEE*. IEEE, 2010, pp. 4304–4307.

[9] C. Quinsac, A. Basarab, and D. Kouamé, "Frequency domain compressive sampling for ultrasound imaging," *Advances in Acoustics and Vibration*, 2012.

[10] T. Chernyakova and Y. C. Eldar, "Fourier-domain beamforming: the path to compressed ultrasound imaging," *Ultrasonics, Ferroelectrics, and Frequency Control, IEEE Transactions on*, vol. 61, no. 8, pp. 1252–1267, 2014.

[11] H. Liebgott, A. Basarab, D. Kouame, O. Bernard, and D. Friboulet, "Compressive sensing in medical ultrasound," in *Ultrasonics Symposium (IUS), 2012 IEEE International*. IEEE, 2012, pp. 1–6.

[12] H. Liebgott, R. Prost, and D. Friboulet, "Pre-beamformed rf signal reconstruction in medical ultrasound using compressive sensing," *Ultrasonics*, vol. 53, no. 2, pp. 525–533, 2013.

[13] M. F. Schiffner and G. Schmitz, "Pulse-echo ultrasound imaging combining compressed sensing and the fast multipole method," in *Ultrasonics Symposium (IUS), 2014 IEEE International*. IEEE, 2014, pp. 2205–2208.

[14] D. L. Donoho, "Compressed sensing," *Information Theory, IEEE Transactions on*, vol. 52, no. 4, pp. 1289–1306, 2006.

[15] E. J. Candès, J. Romberg, and T. Tao, "Robust uncertainty principles: Exact signal reconstruction from highly incomplete frequency information," *Information Theory, IEEE Transactions on*, vol. 52, no. 2, pp. 489–509, 2006.

[16] E. J. Candès and M. B. Wakin, "An introduction to compressive sampling," *Signal Processing Magazine, IEEE*, vol. 25, no. 2, pp. 21–30, 2008.

[17] B. Amizic, L. Spinoulas, R. Molina, and A. K. Katsaggelos, "Compressive blind image deconvolution," *Image Processing, IEEE Transactions on*, vol. 22, no. 10, pp. 3994–4006, 2013.

[18] L. Spinoulas, B. Amizic, M. Vega, R. Molina, and A. K. Katsaggelos, "Simultaneous bayesian compressive sensing and blind deconvolution," in *Signal Processing Conference (EUSIPCO), 2012 Proceedings of the 20th European*. IEEE, 2012, pp. 1414–1418.

[19] S. Boyd, N. Parikh, E. Chu, B. Peleato, and J. Eckstein, "Distributed optimization and statistical learning via the alternating direction method of multipliers," *Foundations and Trends® in Machine Learning*, vol. 3, no. 1, pp. 1–122, 2011.

[20] X. Zhao, C. Chen, and M. Ng, "Alternating direction method of multipliers for nonlinear image restoration problems," *Image Processing, IEEE Transactions on*, vol. 24, no. 1, pp. 33–43, Jan 2015.

[21] A. Antoniadis, D. Leporini, and J.-C. Pesquet, "Wavelet thresholding for some classes of non-Gaussian noise," *STATISTICA NEERLANDICA*, vol. 56, no. 4, pp. 434–453, NOV 2002.

[22] J.-C. Pesquet and N. Pustelnik, "A parallel inertial proximal optimization method," *Pacific Journal of Optimization*, vol. 8, no. 2, pp. 273–305, 2012.

[23] N. Pustelnik, C. Chaux, and J.-C. Pesquet, "Parallel proximal algorithm for image restoration using hybrid regularization," *Image Processing, IEEE Transactions on*, vol. 20, no. 9, pp. 2450–2462, 2011.

[24] N. Pustelnik, J. Pesquet, and C. Chaux, "Relaxing tight frame condition in parallel proximal methods for signal restoration," *Signal Processing, IEEE Transactions on*, vol. 60, no. 2, pp. 968–973, 2012.

[25] P. L. Combettes and J.-C. Pesquet, "Proximal splitting methods in signal processing," in *Fixed-point algorithms for inverse problems in science and engineering*. Springer, 2011, pp. 185–212.

[26] W. Deng, W. Yin, and Y. Zhang, "Group sparse optimization by alternating direction method," in *SPIE Optical Engineering+ Applications*. International Society for Optics and Photonics, 2013, pp. 88 580R–88 580R.

[27] T. T. Do, L. Gan, N. H. Nguyen, and T. D. Tran, "Fast and efficient compressive sensing using structurally random matrices," *Signal Processing, IEEE Transactions on*, vol. 60, no. 1, pp. 139–154, 2012.

[28] J. Yang and Y. Zhang, "Alternating direction algorithms for l1-problems in compressive sensing," *SIAM journal on scientific computing*, vol. 33, no. 1, pp. 250–278, 2011.

[29] J. A. Jensen, "A model for the propagation and scattering of ultrasound in tissue," *Acoustical Society of America. Journal*, vol. 89, no. 1, pp. 182–190, 1991.

[30] A. Florescu, E. Chouzenoux, J.-C. Pesquet, P. Ciuciu, and S. Ciochina, "A majorize-minimize memory gradient method for complex-valued inverse problems," *Signal Processing*, vol. 103, pp. 285–295, 2014.